Research Article

Wenrong Si, Chenzhao Fu, Yue Tian, Jie Chen, Peng Yuan, Zexuan Huang, and Jian Yang*

Numerical study of flow and heat transfer in the channel of panel-type radiator with semi-detached inclined trapezoidal wing vortex generators

https://doi.org/10.1515/phys-2023-0180
received August 29, 2023; accepted January 04, 2024

Abstract: To improve heat dissipation performance of panel-type radiator for transformer, this study investigated the flow and heat transfer characteristics of semi-detached inclined trapezoidal wing vortex generator (SDITW) in a closed channel on the air-side of the radiator. The SDITW was compared with the inclined delta wing (IDW) and inclined trapezoidal wing (ITW) channels. The effects of SDITW relative separation height (e_1/e_2), longitudinal pitch (p_l), blockage ratio ($e/(0.5H)$), and inclination angle (α) were analyzed. First, compared with the IDW and ITW channels, the SDITW channel generates stable corner vortices and produces weaker transverse vortices and lower flow resistance due to the semi-detached structure of the wing. For Re = 5,125–15,375, the overall heat transfer performance (performance evaluation criteria; PEC) of the SDITW channel increases by 0.5–8.9 and 1.7–4.9% as compared with IDW and ITW channels, respectively. Furthermore, for the same $e/(0.5H)$ and α, both the Nusselt number ratio and friction factor ratio of SDITW channel increase as e_1/e_2 and p_l decrease. For p_l = 70 mm, the SDITW channel exhibits a relatively better overall heat transfer performance. For the same e_1/e_2 and p_l, the PEC of SDITW channel is maximum and the overall heat transfer performance is best when $e/(0.5H)$ = 0.3 at Re = 10,250 and α = 30°–60°.

*** Corresponding author: Jian Yang,** MOE Key Laboratory of Thermo-Fluid Science and Engineering, Xi'an Jiaotong University, Xi'an 710049, China, e-mail: yangjian81@mail.xjtu.edu.cn, tel: +86 (29) 82663222, fax: +86 (29) 82663222
Wenrong Si, Chenzhao Fu, Yue Tian, Jie Chen: State Grid Shanghai Electrical Power Research Institute, Shanghai 200437, China
Peng Yuan: Xi'an MaoRong Power Equipment Co., Ltd, Xi'an, 710000, China
Zexuan Huang: MOE Key Laboratory of Thermo-Fluid Science and Engineering, Xi'an Jiaotong University, Xi'an 710049, China

Keywords: panel-type radiator, longitudinal vortex generator, heat transfer enhancement, numerical simulation

Nomenclature

A_f	heat transfer area (m^2)
C_p	specific heat (J/(kg K))
D_h	hydraulic diameter (m)
e	vortex generator height (m)
e_1	vertical distance between trapezoidal wing trailing edge and vertical rib (m)
e_2	vertical distance between trapezoidal wing leading edge and vertical rib (m)
f	friction factor
h	convective heat transfer coefficient ($W/(m^2 \cdot K)$)
H	panel spacing (m)
k	turbulent kinetic energy (m^2/s^2)
L	panel length (m)
L_1	length of entrance section (m)
L_2	length of outlet section (m)
m	mass flow rate (kg/s)
Nu	Nusselt number
p	pressure (Pa)
p_l	longitudinal pitch of vortex generator (m)
Pr	Prandtl number
Re	Reynolds number
T	temperature (K)
u,v,w	velocity components (m/s)
u_m	average inlet velocity (m/s)
W	panel width (m)

Greek letters

α	inclination angle of vortex generator (°)
δ	vortex generator thickness (m)

Open Access. © 2024 the author(s), published by De Gruyter. This work is licensed under the Creative Commons Attribution 4.0 International License.

λ	thermal conductivity (W/(m·K))
λ_{ci}	swirling strength (s^{-1})
μ	kinetic viscosity (Pa s)
ρ	density (kg/m^3)
ω	specific dissipation rate (s^{-1})

Abbreviations

IDW	inclined delta wing
ITW	inclined trapezoidal wing
PEC	performance evaluation criteria
SDITW	semi-detached inclined trapezoidal wing
TEF	thermal enhancement factor

Subscripts

avg	average
in	inlet
out	outlet
t	turbulent
w	wall
0	smooth channel

1 Introduction

Oil-immersed transformers are essential devices for the power system, as they enable efficient transmission, flexible distribution, and safe utilization of electrical energy. To ensure their reliable operation, the heat generated by the internal windings and core must be dissipated promptly to avoid overheating damage. Panel-type radiators are widely used for cooling oil-immersed transformers. Increasing the air velocity between the panels with fans is a typical way to augment heat dissipation. However, when the heat dissipation demand of the transformer is higher, other heat transfer enhancement techniques are also required. Vortex generators are widely used as a passive heat transfer enhancement technique, which usually consist of metal plates attached to the pipe or fin surface at a certain angle of attack concerning the main flow direction. They induce secondary flows (mainly longitudinal vortices) that disrupt or delay the boundary layer development along the wall, enhancing the mixing of hot and cold fluids and thus improving the heat transfer [1].

The flow and heat transfer characteristics in the channel with vortex generators and the effects of their structures have been investigated by many studies. For example, Tiggelbeck *et al.* [2] compared the performance of different types of vortex generators, such as delta wing, rectangular wing, delta winglet pairs, and rectangular winglet pairs. They found that the winglets achieved higher heat transfer than the wing vortex generators but at the expense of higher flow resistance. Fiebig *et al.* [3] reported that the delta wing was the most effective vortex generator in terms of heat transfer enhancement per unit area, followed by delta winglet pairs, while rectangular wing and winglets were less effective. To reduce the pressure drop caused by the vortex generators, some methods such as using holes or curves on the vortex generators or cutting the wing edges are often employed. Skullong *et al.* [4] conducted experimental and numerical studies on the flow and heat transfer performances of perforated rectangular and trapezoidal winglet vortex generators. They found that the perforated jet reduced the vortex intensity and the heat transfer performance, but it also decreased the flow resistance considerably. Hence, the overall heat transfer performance of the perforated winglets was higher than that of the non-perforated winglets. Promvonge and Skullong [5] performed an experimental investigation on heat transfer ducts equipped with perforated winglets.

They showed that the perforated delta winglets enhanced the overall heat transfer performance by 7% over the non-perforated delta winglets. Zhou and Ye [6] introduced a curved trapezoidal winglet vortex generator and tested its flow and heat transfer performances in different flow regimes, which were compared with the conventional rectangular winglet, trapezoidal winglet, and delta winglets. The comparison showed that the delta winglet had the highest overall heat transfer performance in the laminar and transition flow regimes, while the curved trapezoidal winglet had the highest overall heat transfer performance in the turbulent flow regime. Lu and Zhou [7] numerically investigated the flow and heat transfer for a variety of plane and curved vortex generators. They compared the performance of triangular, rectangular, and trapezoidal winglet vortex generators. The results indicated that plane vortex generators had not only higher heat transfer performance but also higher pressure losses. Among the vortex generators, the curved trapezoidal winglets showed the best overall thermal performance. Min *et al.* [8] improved the rectangular winglet by cutting the edges and experimentally investigated its flow and heat transfer performances in a rectangular channel. The results showed that the flow and heat transfer performances of the improved rectangular winglet were better than those of the conventional rectangular winglet. Moreover, the down-sweep

of the longitudinal vortices enhanced the heat transfer, *i.e.*, the distance from the main vortex core of the improved rectangular winglet channel to the heated wall was slightly smaller than that of the conventional rectangular winglet. Dogan and Erzincan [9] experimentally investigated the thermal performance of a novel vortex generator and analyzed the effect of transverse pitch ratio and longitudinal pitch ratio of the vortex generator. The results showed that the maximum thermal enhancement factor (TEF) of the vortex row was 1.59 at the transverse pitch ratio of 0.16 and the longitudinal pitch ratio of 1.5. Demirağ *et al.* [10] experimentally and numerically investigated the heat transfer enhancement and the Darcy friction factor characteristics of a novel-type conical vortex generator in solar air heater and analyzed the effect of various geometrical parameters on the TEF. The TEF is up to 1.316 at optimum geometric conditions. Although many new vortex generators have been designed in the literature, there are still shortcomings in revealing the flow and heat transfer enhancement mechanisms of the new structures, and the analysis of the vortex distribution behind the vortex generator, which plays a crucial role in the flow and heat transfer performance in the channel, is still unclear in most of the available literature.

Vortex generators are widely used in channel heat exchangers such as solar air heaters and fin-tube heat exchangers [11–15]. For example, Promvonge *et al.* [12] conducted an experimental study on the thermal behavior in heat exchanger channels with rib-groove devices on the surface, comparing rib/baffle-groove channels with different rib heights and rib pitches, and the results showed that the baffle-groove yields the highest combined heat transfer performance around 2.14 or about 13% higher than the rib-groove, compared with the thin rib (called "baffle"). Skullong *et al.* [13] experimentally investigated the flow and heat transfer performances of a combined wavy groove-perforated delta wing vortex generator in a solar air heater channel. They found that the overall heat transfer performance of the combined wavy groove-perforated delta wing vortex generator was 12.4 and 45.5% higher than that of the combined wavy groove-delta wing and single wavy groove at different Reynolds numbers. Promvonge *et al.* [14] performed experimental and numerical investigations on the flow and heat transfer characteristics of the combined trapezoidal louvered winglets-wavy groove vortex generator in a solar air heater channel. The louver structure was created by punching square holes at the mass center of the trapezoidal winglet and then bending it over. They found that the overall heat transfer performance of the combined trapezoidal louvered winglets-wavy groove vortex generator was 6.3 and 114% higher than that of the combined trapezoidal winglets-wavy groove and single wavy groove at different Reynolds numbers. Hu *et al.* [15] numerically investigated the effect of staggered concave curved vortex generators on the thermal performance in a wavy finned-tube heat exchanger. The results showed that the Nusselt number and thermal performance factor of the wavy channel with concave curved vortex generator increased by 30.4 and 25.9%, respectively, compared with that of the wavy smooth channel. The application of vortex generators in closed channels for heat transfer augmentation is well-studied in the literature, while the air-side heat dissipation channel of the panel-type radiator for transformers is typically an open channel. The effect of vortex generators on the air-side heat dissipation augmentation of the panel-type radiator has received relatively less attention. Min *et al.* [16] numerically investigated the heat transfer performance of a panel-type radiator with rectangular winglet vortex generators in the air-side channel. They reported that the heat transfer coefficients of the radiator with different sizes of rectangular winglet vortex generators increased by 23.6–32.0% under natural convection conditions. However, they neglected the effect of the air intake at the side of the radiator. Garelli *et al.* [17] numerically investigated the heat transfer performance of a panel-type radiator with delta wing vortex generators in the air-side channel. The vortex generator was placed at a certain height above the panel surface. The results showed that the heat transfer of the radiator improved by 12% under natural convection conditions. They also observed that the air intake at the side of the radiator influenced the longitudinal vortex formation behind the vortex generator, which also affected its heat transfer performance. These studies have demonstrated that the natural convection heat dissipation of the panel-type radiator can be significantly improved by arranging vortex generators in the air-side channel. However, the forced convection heat transfer in the air-side vortex generator channel of the panel-type radiator was still not reported in the literatures.

Based on the above analysis, this study intends to investigate the forced convection heat transfer in the air-side vortex generator channel of the panel-type radiator for the transformer with numerical method. To eliminate the adverse effect of the air intake from the side of the radiator, the baffle plates on both sides of the panel-type radiator are added to form a closed air flow channel. Improvement of trapezoidal wing in literature review has a greater potential to improve the heat transfer performance of the channel, while the delta wing has a simple structure and is more studied and applied. In the present study, the traditional inclined trapezoidal wing (ITW) is structurally improved and the semi-detached inclined trapezoidal wing vortex generators (SDITW) were designed and arranged on the surface of the radiator. The SDITW

is obtained by cutting the trailing edge of the ITW, which can separate the ITW from the radiator surface and enhance the heat transfer in the channel while reducing the flow resistance. First, the flow and heat transfer characteristics of SDITW in closed channels at the air-side of the panel radiator were investigated and the performance of SDITW was compared with that in the inclined delta wing (IDW) and ITW channels with the same geometrical configuration. Second, the effects of SDITW relative separation height (e_1/e_2), longitudinal spacing (p_l), blockage ratio ($e/(0.5H)$), and inclination angle (α) on the flow and heat transfer in SDITW channels were analyzed in detail. This study can act as an important reference for the heat transfer enhancement on the air-side of the panel-type radiator used for transformers and structure design of corresponding vortex generator.

2 Physical model and computational methods

2.1 Physical model

A simplified physical model is developed to investigate the heat transfer performance of the panel-type radiator, based on the models reported in previous studies [16,17]. Figure 1 shows the panel-type radiator model, where Figure 1(a) presents the vertical closed channels formed by baffles on both sides of the radiator. The baffles avoid side air intake, which affects the formation of longitudinal vortices in the edge region [z17]. Figure 1(b) shows the radiator unit extracted from the panel-type radiator. Considering the symmetry of the geometry and physical model, a quarter of the air channel of the radiator unit is simplified as the computational domain, as shown in Figure 1(c). The physical model simplifies the air passage as a rectangular duct, neglecting the trapezoidal oil channel structure on the panel surface [16]. This simplification is also adopted in other studies [18,19]. In the physical model, the surfaces at $y = 0$ and $z = H/2$ are symmetrical. The bottom surface of the channel is isothermal, and the side wall is no-slip and adiabatic wall. The dimensions of the flow channel are as follows: the spacing between panels is $H = 45$ mm, the width of the panel is $W = 450$ mm, the length is $L = 1{,}524$ mm, and the hydraulic diameter is 81.82 mm. The flow channel dimensions are consistent with the panel dimensions, detailed dimensions can be found in the study by Garelli *et al.* [17]. Since most of the area in the flow channel is fully developed, the entry and exit sections are set according to the ASHARE standard to eliminate inlet and outlet effects [20]. The length of the inlet section L_1 should be larger than $5\sqrt{WH}$ and the length of the outlet section should be larger than $2.5\sqrt{WH}$. Therefore, L_1 is set as 800 mm and L_2 is set as 500 mm.

In this study, the SDITW vortex generators are attached to the panel surface to enhance the convective heat transfer of the air-side in the panel-type radiator. Figure 2 shows the arrangement and geometric structure of the SDITWs. The

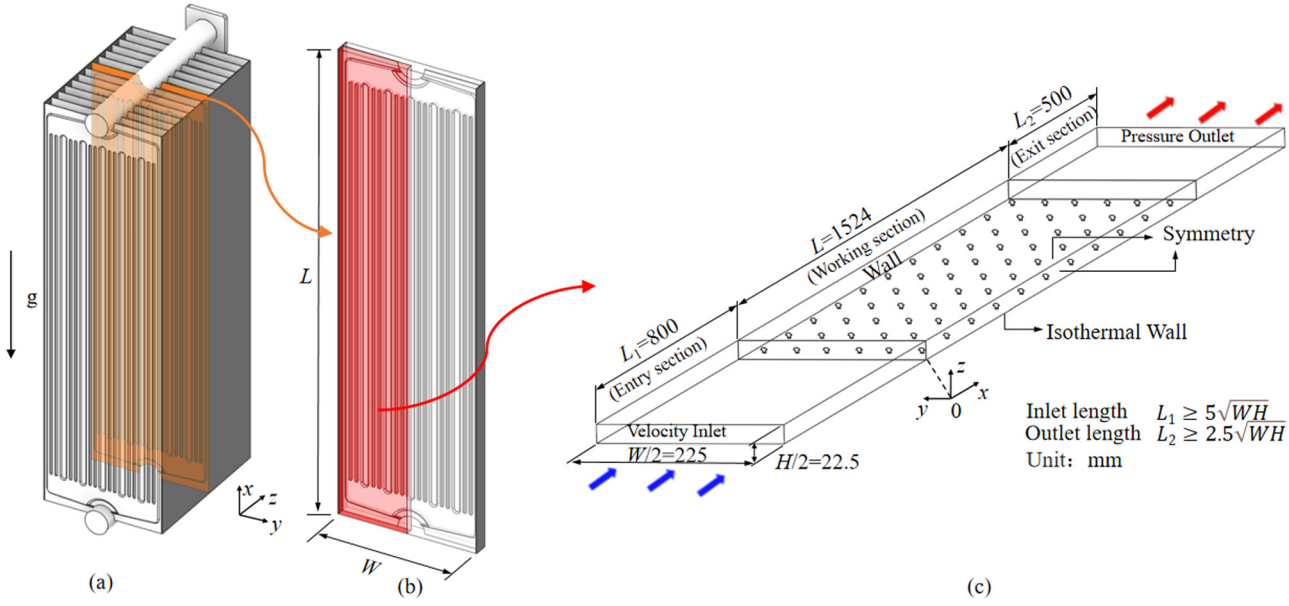

Figure 1: Panel-type radiator and simplified physical model of air channel between panels. (a) Panel-type radiator. (b) Radiator unit. (c) Computational domain.

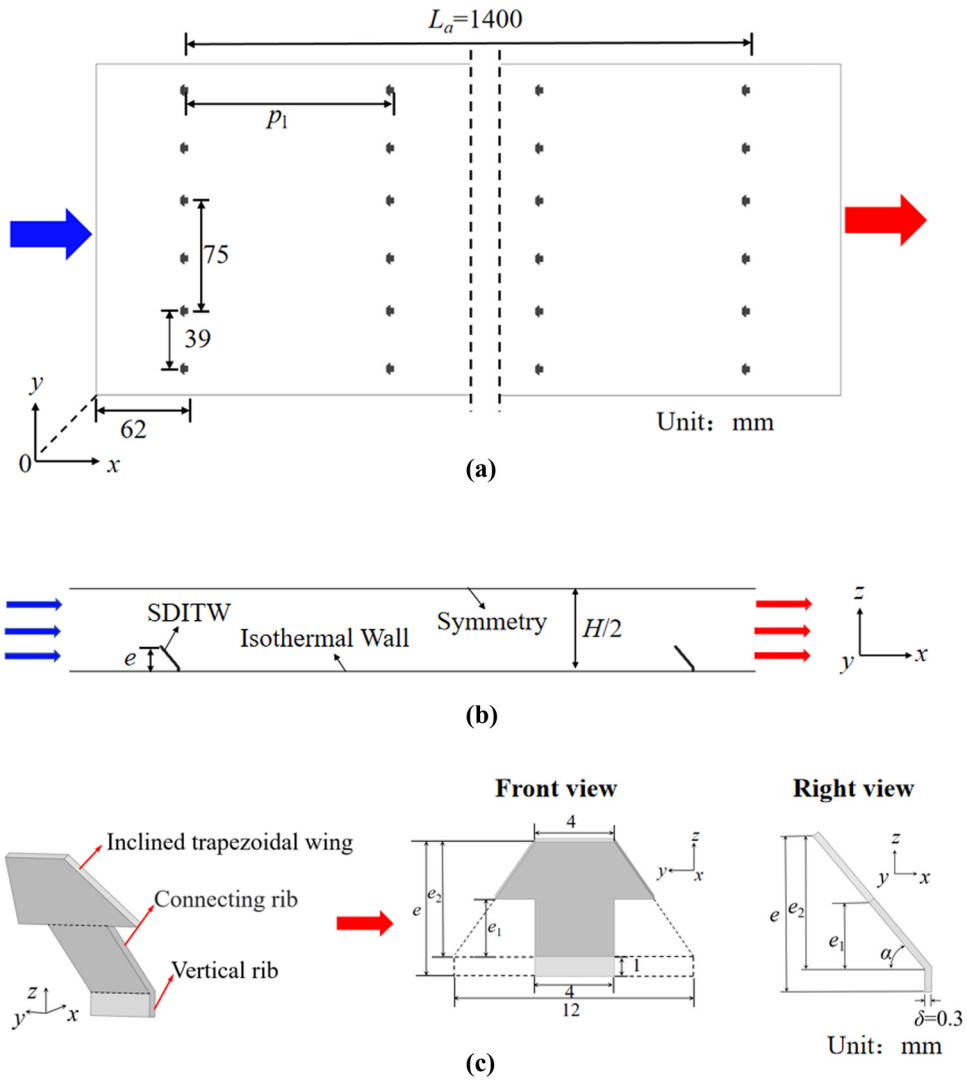

Figure 2: Geometry and arrangement of SDITWs. (a) Top view. (b) Side view. (c) SDITW.

SDITWs are uniformly arranged along the x-direction with p_1 as the longitudinal pitch, and the first and last rows of vortex generators are 62 mm away from the edge of the channel. With the trapezoidal oil channel structure of ref. [16], the SDITWs are mounted along the y-direction corresponding to the locations of the oil channel bumps.

The SDITW is composed of an ITW, a vertical rib, and a connecting rib. The ITW deflects the fluid to scour the heated wall and generates longitudinal vortices. The vertical rib and connecting rib can enhance the disturbance and fix the SDITW on the heated wall narrow oil channel bump. According to the delta wing vortex generator design in the study by Bekele *et al.* [21] and actual panel structural features [16], the dimension parameters of SDITW is designed. The geometrical parameters of the SDITW are as follows: the vertical rib height is 1 mm, the width is 4 mm, the leading edge width of the ITW is 4 mm, the vertical distance between the trailing edge and vertical rib is e_1, the vertical distance between the leading edge and vertical rib is e_2, the total height of the SDITW is e, and its thickness δ is 0.3 mm.

To analyze the flow and heat transfer characteristics of the SDITW, four main geometric parameters are selected for parametric analysis, namely, the relative separation height (e_1/e_2), the longitudinal pitch (p_1), the inclination angle (α), and the blockage ratio ($e/(0.5H)$). These parameters are listed in Table 1.

2.2 Governing equations and computational methods

The working fluid in this study is air. Due to small variation in air temperature, the air properties are assumed to be constant and 303.15 K is set as the qualitative temperature.

Table 1: Geometric parameters of SDITW

Parameters	Values
e_1/e_2	0, 0.25, 0.5, and 0.75
p_l (mm)	40, 50, 70, 100, and 140
α/(°)	20, 30, 40, 50, and 60
e/(0.5H)	0.15, 0.3, 0.45, and 0.6

Radiation and natural convection of air are neglected. The flow and heat transfer processes are described by the mass, momentum, and energy equations [22] as follows:

$$\frac{\partial \rho u_i}{\partial x_i} = 0, \tag{1}$$

$$\frac{\partial}{\partial x_j}(\rho u_i u_j) = -\frac{\partial p}{\partial x_i} + \frac{\partial}{\partial x_j}\left[(\mu + \mu_t)\left(\frac{\partial u_i}{\partial x_j} + \frac{\partial u_j}{\partial x_i}\right)\right], \tag{2}$$

$$\frac{\partial}{\partial x_j}(\rho u_j c_p T) = \frac{\partial}{\partial x_j}\left[\left(\lambda + \frac{\mu_t c_p}{Pr_t}\right)\frac{\partial T}{\partial x_j}\right], \tag{3}$$

where u_i is the velocity component in the i-direction. ρ, μ, λ, and c_p are the density, kinetic viscosity, thermal conductivity, and specific heat capacity of the fluid, respectively. The turbulent Prandtl number is $Pr_t = 0.85$, and the turbulent viscosity μ_t is calculated by the turbulence model.

The SST k–ω turbulence model is adopted in this study, which combines the advantages of both the k–ω and k–ε models. The k–ω model is applied in the boundary layer, while the k–ε model is applied in the turbulent region away from the wall, which avoids the sensitivity of the k–ω model to the inlet free-stream turbulence properties. The turbulence model has high accuracy and reliability in adverse pressure gradient and separated flow conditions. Moreover, the SST k–ω model has also been used by several researchers for the curvature flow similar to this study, and showed good agreement with the experimental results [23–25].

The SST k–ω model transport equations are as follows:

$$\frac{\partial}{\partial x_j}(\rho k u_j) = \frac{\partial}{\partial x_j}\left(\Gamma_k \frac{\partial k}{\partial x_i}\right) + G_k - Y_k, \tag{4}$$

$$\frac{\partial}{\partial x_j}(\rho \omega u_j) = \frac{\partial}{\partial x_j}\left(\Gamma_\omega \frac{\partial \omega}{\partial x_i}\right) + G_\omega - Y_\omega. \tag{5}$$

For a detailed discussion of the model, please refer to the study by Menter [26].

The governing equations are solved based on the finite volume method using the CFD commercial software Ansys Fluent. The pressure-velocity coupling is performed by the SIMPLE algorithm, and the second-order upwind scheme is applied for the convective terms in the momentum, energy, turbulent kinetic energy, and specific dissipation rate equations to ensure the computational accuracy. The convergence criteria for the continuity and momentum equations are set to 10^{-4}, and the convergence criteria for the energy equation is set to 10^{-8}. A uniform velocity profile and a uniform temperature of 303.15 K are given at the inlet. The pressure outlet boundary condition is used at the outlet. A symmetry boundary condition is applied on the plane of y = 0 and $z = H/2$. The heated wall temperature in the test section is assumed to be 340 K, which are similar to those in the study by Garelli *et al.* [17]. No-slip wall conditions are applied on the channel walls.

In this study, some of the parameters are defined as follows:

Hydraulic diameter:

$$D_h = \frac{2WH}{W + H}. \tag{6}$$

Reynolds number [27]:

$$Re = \frac{\rho u_m D_h}{\mu}, \tag{7}$$

where u_m is the average inlet velocity.

Darcy friction factor [27]:

$$f = \frac{\Delta p}{(0.5\rho u_m^2)(L/D_h)}, \tag{8}$$

where Δp and L are the pressure drop and channel length of the test section, respectively.

Nusselt number [27]:

$$Nu = \frac{hD_h}{\lambda}, \tag{9}$$

where the convective heat transfer coefficient h of the heated wall is defined as follows:

$$h = \frac{mC_p(T_{out} - T_{in})}{A_f(T_w - T_{avg})}, \tag{10}$$

$$T_{avg} = \frac{T_{in} + T_{out}}{2}, \tag{11}$$

where m is the inlet mass flow rate, T_{in} and T_{out} are the average inlet and outlet temperatures, respectively, and A_f is the heat transfer area.

The performance evaluation criterion (PEC) [27] is defined as the ratio of Nusselt number of the enhanced heat transfer channel (Nu) to Nusselt number of the smooth channel (Nu_0) at equal pumping power and is expressed as follows:

$$PEC = \frac{Nu/Nu_0}{(f/f_0)^{1/3}}, \tag{12}$$

where Nu_0 and f_0 represent the average Nusselt number and friction factor for the smooth channel, respectively. It can be seen that PEC is a comprehensive evaluation index of heat transfer enhancement effect and pumping power loss cost. When PEC is greater than 1, the positive benefit of heat transfer enhancement can be achieved, indicating that the heat transfer enhancement effect is greater than the cost of pumping power loss.

3 Grid independence test and model validations

3.1 Grid independence test

To ensure the accuracy of the numerical simulation, the computational mesh is first examined for grid independence. A 3D hybrid mesh consisting of hexahedral and polyhedral cells is generated using Fluent Meshing software. And the mesh near the wall is refined to capture the flow and heat transfer phenomena within the boundary layer, as shown in Figure 3. In this study, the SDITW vortex generator with an inclination angle (α) of 30°, a relative separation height (e_1/e_2) of 0.5, a blockage ratio ($e/(0.5H)$) of 0.3, and a longitudinal pitch (p_l) of 70 mm are selected. Six sets of computational grids are generated, and the Nu and f values under different grids are listed in Table 2. When the grid number increases from 6,238,234 (Case 4) to 9,128,832 (Case 5), the relative deviations of Nu and f are 0.06 and 0.64%, respectively. It indicates that the calculation results under this grid (Case 4) setting are grid independent. Therefore, the grid setting of Case 4 is adopted in this study.

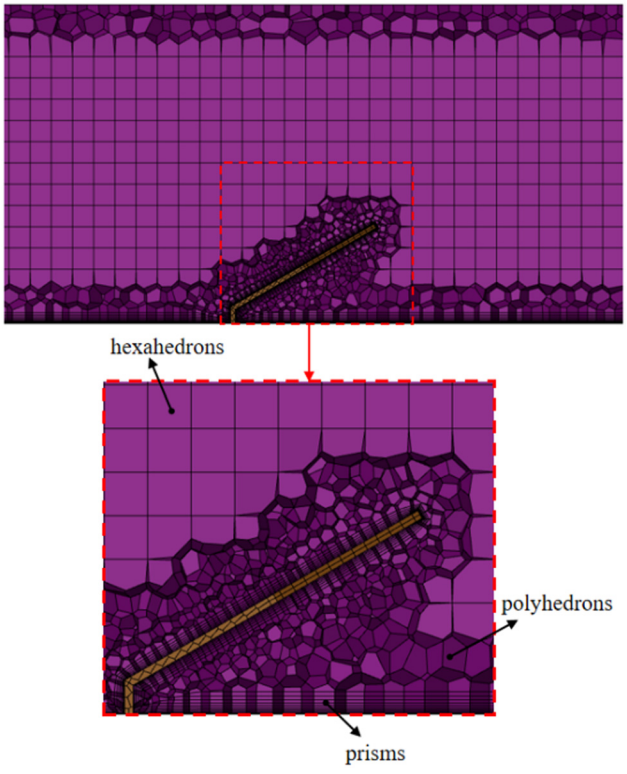

Figure 3: Computational grid.

3.2 Model validations

To verify the accuracy of the numerical model and computational method, the simulation results are compared with the empirical correlation formula and experimental results. Figure 4(a) shows the comparison between the present results in the smooth channel and the predicted results from the empirical correlations (13) and (14) as reported by Incropera *et al.* [28]. The two results agree well with each other, and the average deviations of Nu and f are 1.8 and 5.1%, respectively. It indicates that the numerical model used in this study can accurately simulate the flow and heat transfer process in the smooth channel. Figure 4(b) compares the simulation results with the experimental results of the study by Skullong *et al.* [13] for the case with delta wing vortex generators. Due to the similarities between the delta wing vortex generator and SDITW, the experimental results of the study by Skullong *et al.* [13] can be used to further validate the accuracy of the numerical model proposed in this study. As shown in Figure 4(b), the two results agree well with each other, and the average deviations of Nu and f are 5.1 and 6.2%, respectively. It indicates that the numerical model can capture the effect of the delta wing vortex generator on the flow and heat transfer. Therefore, the numerical model and computational method used in this study are reliable, which can be used for the subsequent analysis of flow and heat transfer characteristics of SDITW channel.

Table 2: Variations in Nu and f with different computational grids (Re = 5,125)

Case	Grid number	Nu	f
1	1,664,183	73.63	0.1111
2	2,693,174	77.57	0.1169
3	3,755,845	79.96	0.1242
4	6,238,234	81.40	0.1251
5	9,128,832	81.35	0.1259
6	16,734,914	82.19	0.1268

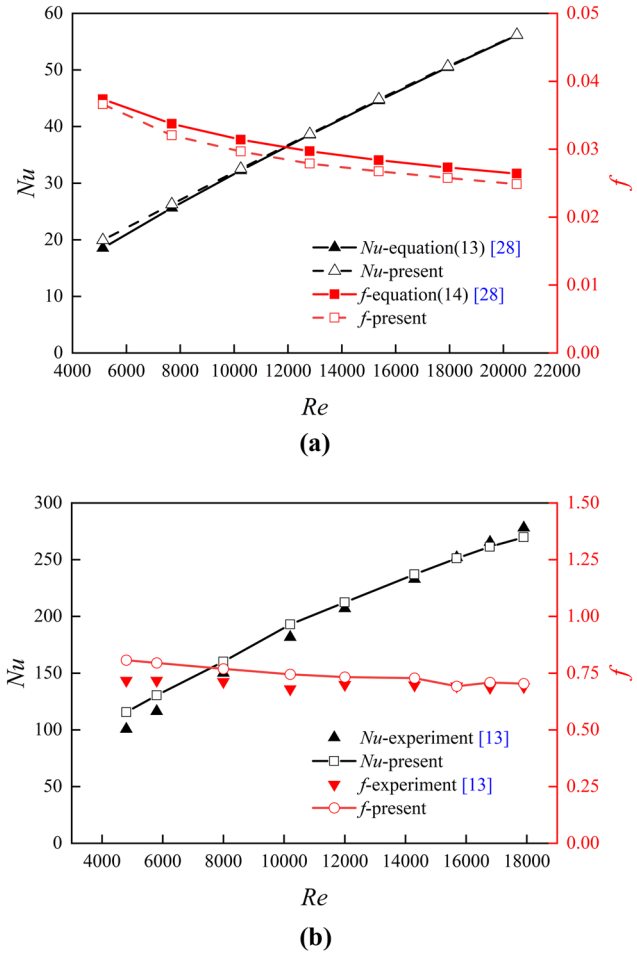

Figure 4: Model validation for Nu and *f*. (a) smooth channel. (b) Delta wing vortex generator channel.

$$\mathrm{Nu} = 0.023\mathrm{Re}^{0.8}\mathrm{Pr}^{0.4}, \tag{13}$$

$$f = 0.316\mathrm{Re}^{-0.25}. \tag{14}$$

4 Results and discussion

In this study, the flow and heat transfer characteristics of the SDITW vortex generator in a closed channel on the air-side of the panel-type radiator are numerically investigated. The flow characteristics and heat transfer enhancement mechanism of the SDITW were revealed by comparing with the IDW and the ITW with the same geometric configuration. The effects of relative separation heights (e_1/e_2), longitudinal pitch (p_l), blockage ratio ($e/(0.5H)$), and inclination angle (α) on the flow and heat transfer for the SDITW channel were analyzed in detail.

4.1 Comparison of flow and heat transfer performances in different vortex generator channels

Three kinds of vortex generators with the same geometric configuration are selected for comparison and analysis. The relative separation height (e_1/e_2), longitudinal pitch (p_l), blockage ratio ($e/(0.5H)$), and inclination angle (α) are fixed at 0.5, 70 mm, 0.3, and 50°, respectively. The flow and heat transfer characteristics in the channel of the SDITW vortex generator are compared with those of the traditional IDW and the ITW. Figure 5 shows the specific geometric structures of three vortex generators, which have the same height and pitch angle. The bottom edges of the IDW and ITW are equal in width, and the SDITW is obtained by cutting the trailing edge of the ITW.

Figure 6 shows the streamline and the vortex intensity distributions at different *yz* planes between two adjacent

vortex generators at the center of the channel for Re = 5,125. The vortex intensity is quantified by the swirling strength λ_{ci}, which is the imaginary part of the eigenvalue of the velocity gradient tensor. The swirling strength λ_{ci} can visualize the vortex and identify its core and size. The detailed definition and description of the swirling strength λ_{ci} can be found in the study by Zhou *et al.* [29]. The streamline distribution in Figure 6 shows that three vortex structures are generated behind the vortex generator, including the main vortex, corner vortex, and induced vortex. The main vortex is located in the central region of the channel, which promotes the mixing of hot and cold fluid. The corner vortex is located in the near-wall region, which enhances the wall convection heat transfer, and the induced vortex is induced by the primary vortex, which is distributed in the edge near-wall region. The IDW and ITW form the corner vortex at x = 767 mm and x = 769.5 mm, respectively, and then the corner vortex disappears rapidly, while the SDITW forms the corner vortex at x = 764.5 mm and it can maintain at a certain distance. The vortex intensity distribution indicates the location and intensity of the vortex. Generally, the vortex intensity in the near-wall region is higher than that in the central region, and the vortex intensity decreases gradually with the increase in the flow distance. The vortex intensity distribution of SDITW also shows that the corner vortex in the near-wall region spreads to both sides as the flow distance increases. Among the three vortex generators, the ITW shows the widest influence range of vortex spreading and the SDITW shows the narrowest influence range, which is related to the transverse span of the vortex generator. The average vortex intensity $\lambda_{ci,ave}$ of the three vortex generator channels shows different trends along the flow direction. At the initial position (x = 764.5 mm), the ITW channel has the highest $\lambda_{ci,ave}$, followed by the IDW channel and the SDITW channel. However, as the flow moves downstream, $\lambda_{ci,ave}$ of the IDW channel and the ITW channel decreases sharply, while that of the SDITW channel changes slightly. In the range of x = 764.5 mm to x = 797 mm, $\lambda_{ci,ave}$ of the IDW, ITW, and SDITW channel reduces by 73.5, 70.93, and 53.74%, respectively. This indicates that the SDITW channel can preserve better flow mixing capability than the other two channels. Moreover, the SDITW channel has the largest local vortex intensity, followed by the ITW channel, and the IDW channel has the smallest local vortex intensity. Larger local vortex intensity means better heat transfer performance, which means the SDITW channel may have the best heat transfer performance among the three vortex generators.

To visualize the longitudinal vortex structure for the SDITW channel and compare it with the IDW and ITW channels, the Q criterion vortex identification method is used for analysis. The Q criterion is defined as follows [30]:

$$Q = -\frac{1}{2}\left[\left(\frac{\partial u}{\partial x}\right)^2 + \left(\frac{\partial v}{\partial y}\right)^2 + \left(\frac{\partial w}{\partial z}\right)^2\right] - \left[\frac{\partial u}{\partial y}\frac{\partial v}{\partial x} + \frac{\partial u}{\partial z}\frac{\partial w}{\partial x} + \frac{\partial v}{\partial z}\frac{\partial w}{\partial y}\right]. \tag{15}$$

Figure 7 shows the Q criterion distribution in the channel of different vortex generators. Regions with Q values greater than 1 indicate the presence of longitudinal vortices in the flow field. As shown in Figure 7(a)–(c), longitudinal vortices are generated behind all three types of vortex generators. Near the vortex generator, the vortex intensity is high and it decreases as the flow distance increases. When the fluid flows through multiple vortex generators, the longitudinal vortex gradually strengthens and reaches a steady state after passing through the third vortex generator. Then, the longitudinal vortex varies periodically along the flow direction. In different vortex generator channels, the main vortex behind IDW and ITW, and the main vortex and corner vortex behind the SDITW can be clearly observed. The induced vortex is small and cannot be easily observed. As shown in Figure 7(d), the Q value of the main vortex on both rear sides of SDITW is low, which is similar to the IDW and ITW. However, its Q value of the corner vortex near the central axis is high. The

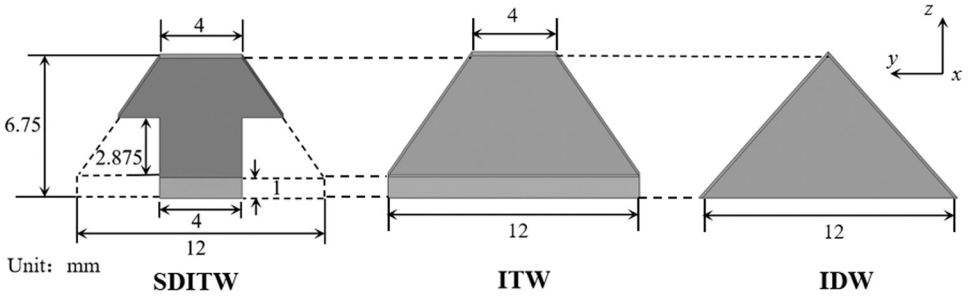

Figure 5: Front view of different vortex generators.

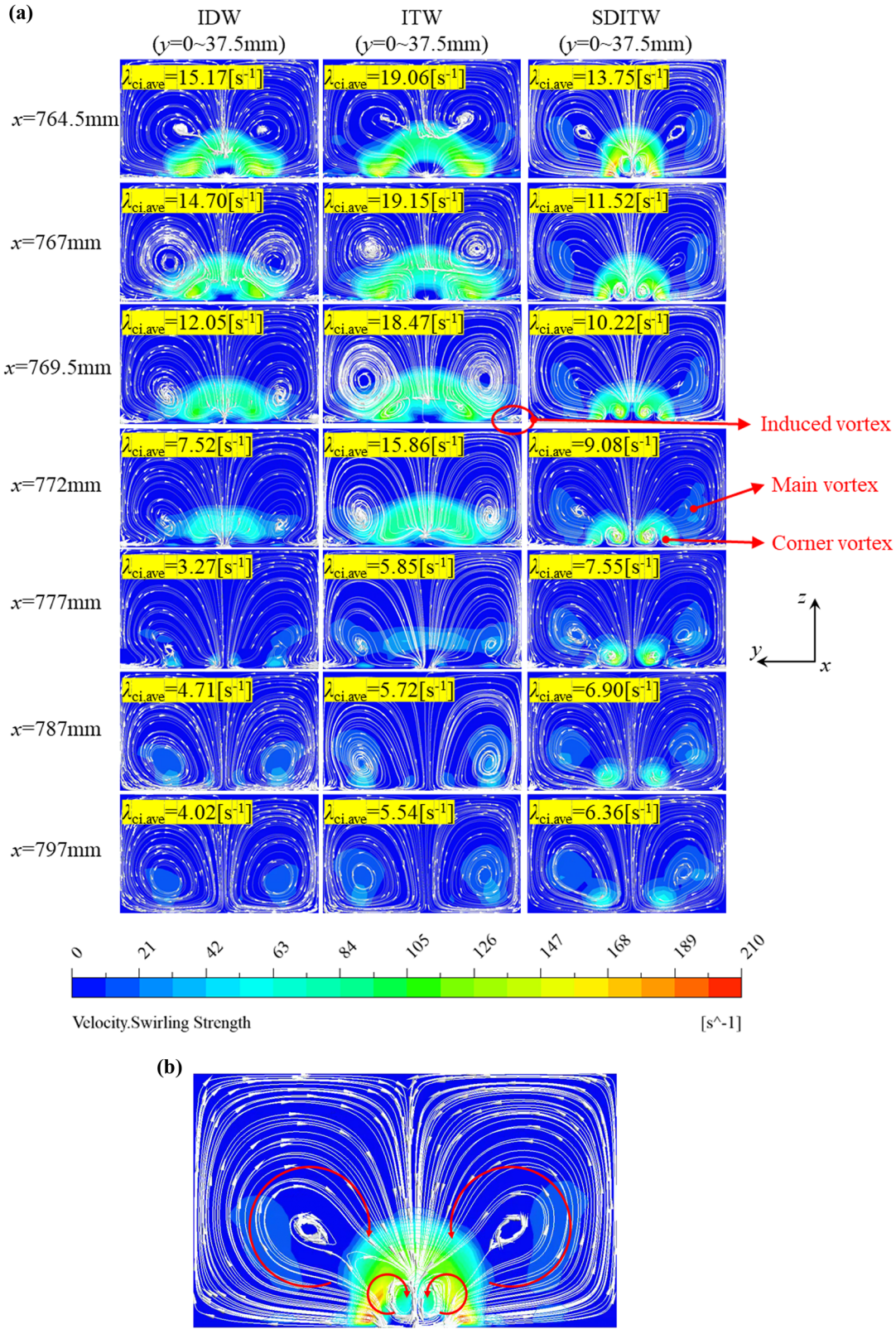

Figure 6: (a) Velocity streamlines and vortex intensity distributions in different *yz* planes between adjacent vortex generators in the middle of the channel and (b) detailed view of the velocity streamlines and vortex intensity distributions in the *yz* plane at x = 764.5 mm in the SDITW channel (Re = 5,125).

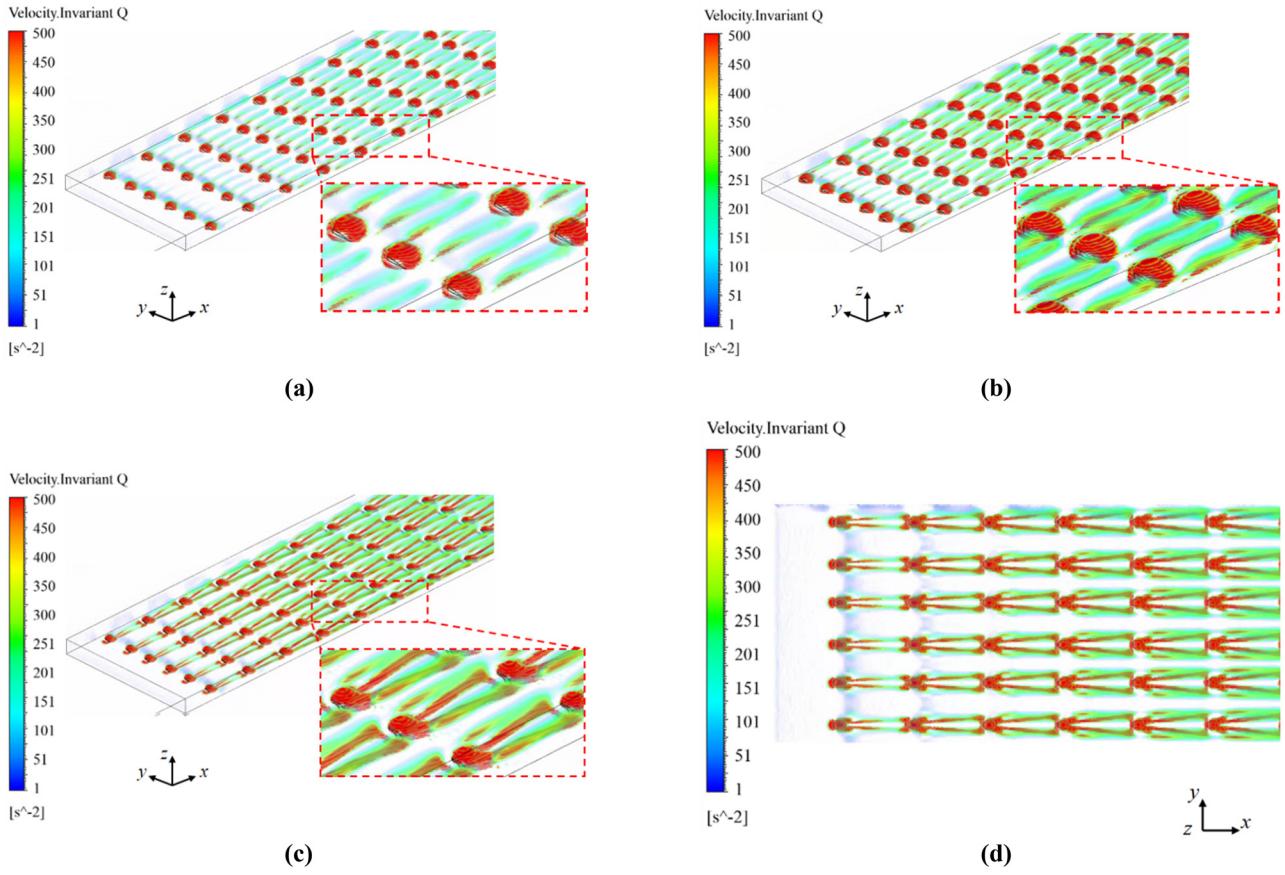

Figure 7: Distributions of vortex *Q* criterion in different vortex generator channels (Re = 5,125). (a) Axial side view of IDW channel. (b) Axial side view of the ITW channel. (c) Axial side view of the SDITW channel. (d) Top view of SDITW channel.

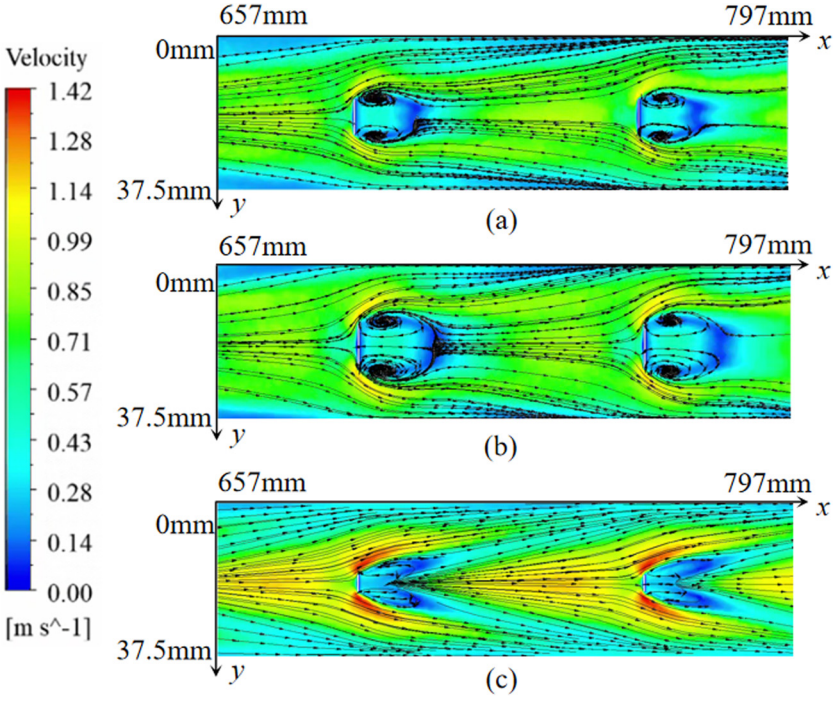

Figure 8: Local streamline and velocity distributions at *xy* plane (*z* = 2 mm) in different vortex generator channels (Re = 5,125). (a) IDW channel. (b) ITW channel. (c) SDITW channel.

corner vortex exists stably in the SDITW channel and gradually spreads to both sides as the flow distance increases. Therefore, compared with the IDW and ITW, the longitudinal vortex generated in the SDITW channel is stronger.

Figure 8 shows the local streamline and velocity distributions at *xy* plane (z = 2 mm) in different vortex generator channels at Re = 5,125. It can be seen that a pair of strong transverse vortices are generated behind the IDW and ITW, which can cause strong backflow and form a low-speed recirculation zone. Compared with the ITW, the SDITW channel has weaker transverse vortices and a smaller low-speed recirculation zone due to its semi-detached structure.

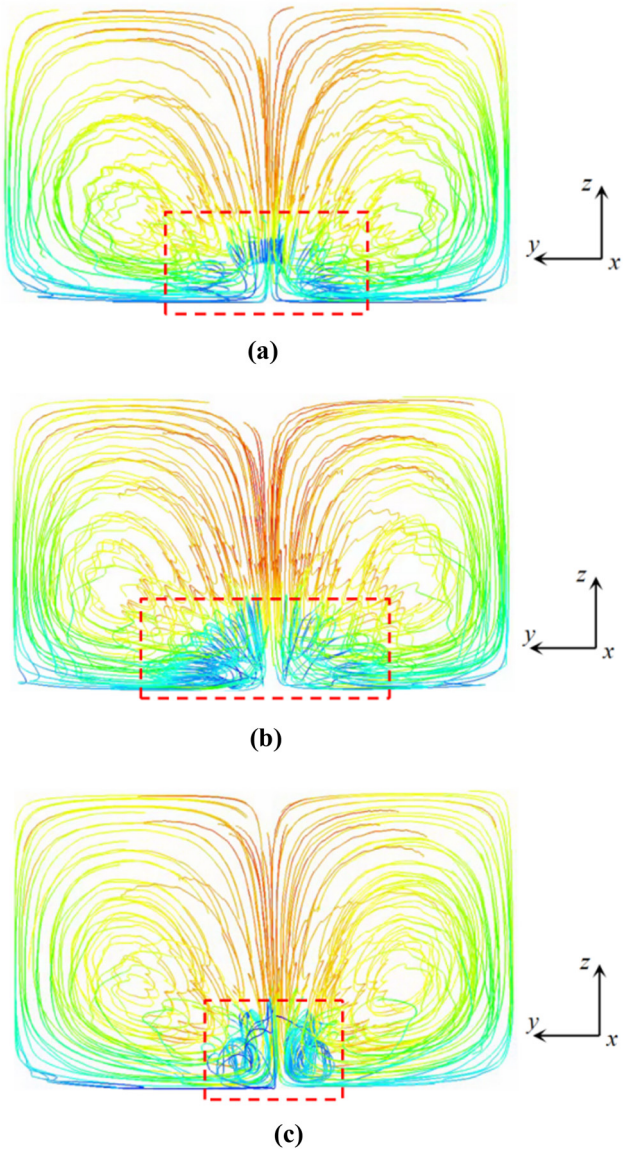

Figure 9: Local 3D streamline distributions of different vortex generator channels (Re = 5,125). (a) Front view of the IDW channel. (b) Front view of the ITW channel. (c) Front view of the SDITW channel.

In addition, the flow velocity in the high-speed region in the SDITW channel is obviously higher than that in the IDW and ITW channels, which is beneficial to enhance convective heat transfer in the near-wall region of the channel.

Figure 9 shows the distributions of local three-dimensional streamline in different vortex generator channels. It can be seen that, the IDW and ITW generate more transverse vortices due to their larger transverse spans and projection areas. However, the SDITW generates fewer transverse vortices and forms a pair of longitudinal vortices. It indicates that the semi-detached structure of SDITW can reduce transverse vortices and flow resistance while increase the longitudinal vortex effect.

Figure 10 shows the local temperature and velocity vector distributions of different channels at *yz* plane (x = 782 mm). As shown in Figure 10, near the vortex generators, the temperature field shows an alternating distribution of hot and cold fluids. This is due to the influence of the longitudinal vortex, which causes the cold fluid behind the vortex generator moving from the core region towards the heated surface to absorb heat and then diffuse to the side regions. Meanwhile, the hot fluid between the two transverse adjacent vortex generators moves from the wall to the core region. In addition, the ITW and SDITW channels show more uniform temperature distributions as compared to the IDW channel, which indicates they would have better heat transfer performance. The temperature distributions in the ITW and SDITW channels are similar, but thinner thermal boundary layer is observed near the wall in the middle region between two adjacent ITWs, which represents higher heat transfer rate. This phenomenon is due to the large transverse span of the ITW, which

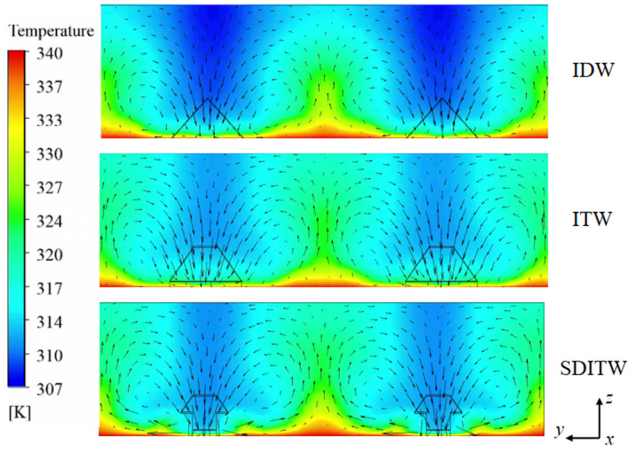

Figure 10: Local temperature and velocity vector distributions at *yz* plane (x = 782 mm) (Re = 5,125).

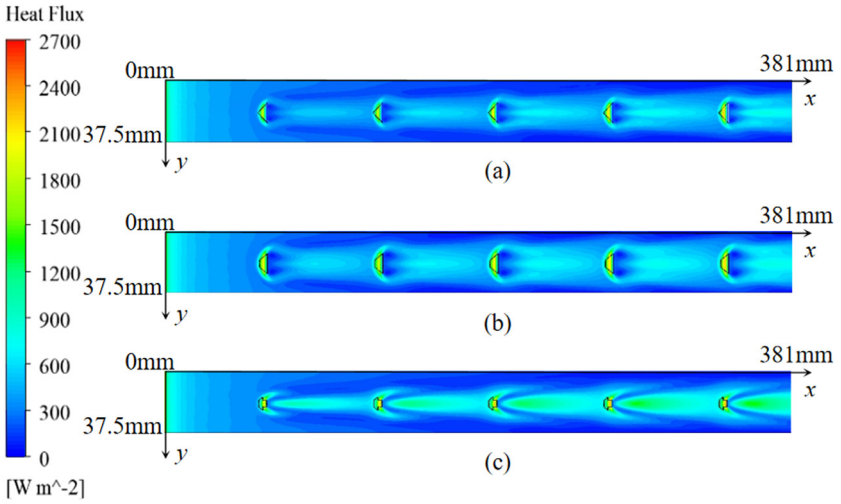

Figure 11: Local heat flux distribution at the heating surface of different vortex generator channels (Re = 5,125). (a) IDW channel. (b) ITW channel. (c) SDITW channel.

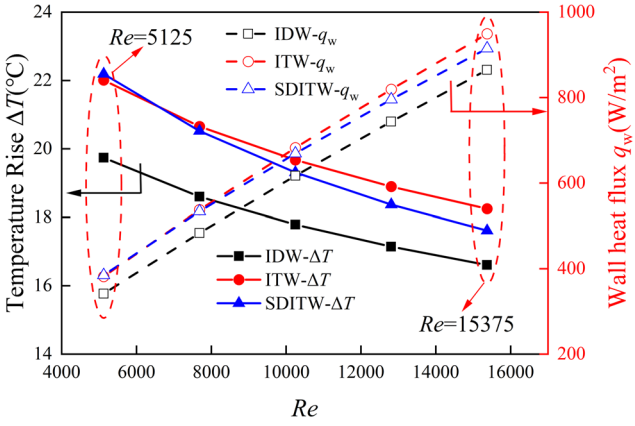

Figure 12: Variations in heat flux on the heating plate and the temperature rise between the inlet and outlet of different vortex generator channels with Re.

can induce longitudinal vortices and lead to significant transverse effect on the flow and heat transfer.

Figure 11 shows the local heat flux distribution at the heating surface of different vortex generator channels. It is obvious that the IDW and ITW channels exhibit low local heat transfer in the wake region of the vortex generators, which is attributed to the existence of large transverse vortices. On the other hand, in the SDITW channel, the semi-detached structure of the SDITW diminishes the transverse vortices and generates a pair of corner vortices, which will enhance the local heat transfer behind the vortex generator.

Figure 12 shows the variations in the heat flux on the heating plate and the temperature rise between the inlet and outlet of different vortex generator channels with Re. It shows that the temperature rise decreases, while the heat flux increases as Re increases, which indicates the improvement of heat transfer. The temperature rise and heat flux of ITW and SDITW channels are higher than the IDW channel, indicating that the heat transfer performances of ITW and SDITW channel are better. The heat transfer performances of the ITW and SDITW channels are close with each other, where the SDITW channel shows better heat transfer performance at low Re (Re = 5,125), while the ITW channel shows better heat transfer performance at high Reynolds number (Re = 15,375). According to previous analysis, it reveals that the SDITW channel exhibits higher local heat transfer performance behind the vortex generator, but lower heat transfer performance in the near-wall zone in the middle of the adjacent vortex generator, due to the smaller transverse influence range of the longitudinal vortex. Conversely, the ITW channel shows the opposite trend, resulting in different heat transfer performances between ITW and SDITW channels at different Re. In addition, it is also found that the effect of heat transfer in the near-wall region in the middle of the adjacent vortex generator is gradually obvious as Re increases.

Figure 13 shows the variations in the Nusselt number ratio (Nu/Nu_0), friction factor ratio (f/f_0), and PEC with Reynolds number (Re) in different vortex generator channels. The Nu/Nu_0 indicates the enhancement of heat transfer in the vortex generator channel relative to the smooth channel. The f/f_0 represents the increase in pressure loss, and the PEC evaluates the overall thermal performance of the vortex generator channel. As shown in Figure 13, the heat transfer enhancement (Nu/Nu_0) of the

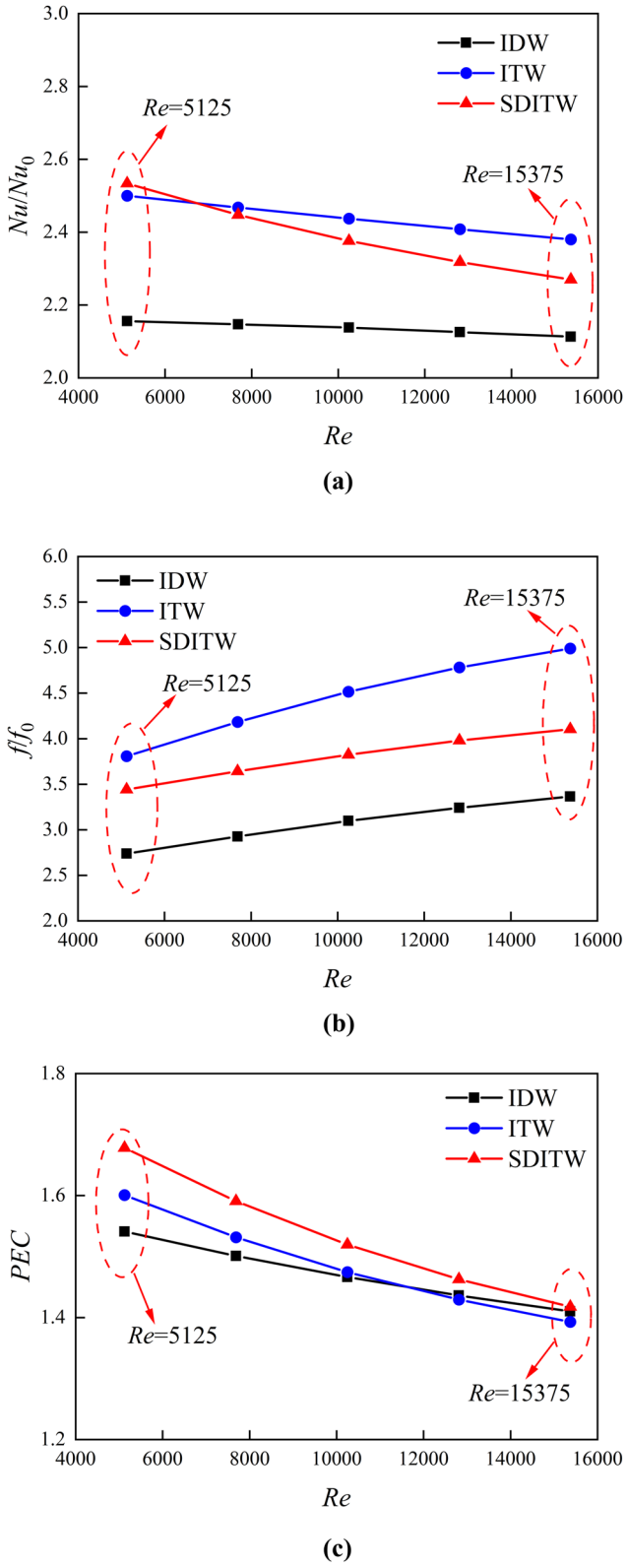

Figure 13: Variations in Nu/Nu_0, f/f_0, and PEC with Re in different vortex generator channels. (a) Nu/Nu_0. (b) f/f_0. (c) PEC.

vortex generator decreased, the pressure loss (f/f_0) increased, and the overall heat transfer performance (PEC) decreased as the Reynolds number (Re) increased. The IDW channel showed the lowest Nu/Nu_0 and PEC, which indicates that it has poor flow and heat transfer performance. The heat transfer enhancement (Nu/Nu_0) is increased by 12.6–15.69% and the pressure loss (f/f_0) is increased by 39.1–48.3% in the ITW channel as compared to the IDW channel at different Re. Due to the larger projected area of the ITW and stronger disturbance effect, it has a better heat transfer performance and higher flow resistance. Moreover, the overall heat transfer performance (PEC) of the ITW channel is 3.9% higher than that of the IDW channel at low Reynolds number (Re = 5,125), whereas it is lower than that of the IDW channel at high Reynolds number (Re = 15,375). At different Reynolds numbers, the heat transfer enhancement (Nu/Nu_0) of the SDITW channel is 7.4–17.5% higher than that of the IDW channel, while its pressure loss (f/f_0) is only 21.9–25.7% higher. The overall heat transfer performance (PEC) of the SDITW channel is 0.5–8.9% higher than that of the IDW channel and 1.7–4.9% higher than that of the ITW channel. The SDITW channel has better overall heat transfer performance than the IDW and ITW channels at different Reynolds numbers. Therefore, the SDITW is more efficient than the delta wing (IDW) and trapezoidal wing (ITW).

4.2 Effect of geometric parameters on the flow and heat transfer performances of the SDITW channel

4.2.1 Effect of relative separation height and longitudinal pitch

Figure 14 presents the temperature and vortex intensity distributions at yz plane (x = 772 mm) in the SDITW channel with different relative separation heights (e_1/e_2) when Re = 10,250, p_1 = 70 mm, $e/(0.5H)$ = 0.3, and α = 30°. As the e_1/e_2 decreases, the projected area of the vortex generator increases, and the flow disturbance is enhanced. The intensity and influence range of the main, corner, and induced vortices are increased, and the average vortex intensity rises from 19.8 to 34.1 s^{-1}. The corner vortex in the near-wall region enhances the convective heat transfer near the wall, and the main vortex in the core region promotes the mixing of hot and cold air. Therefore, as the e_1/e_2

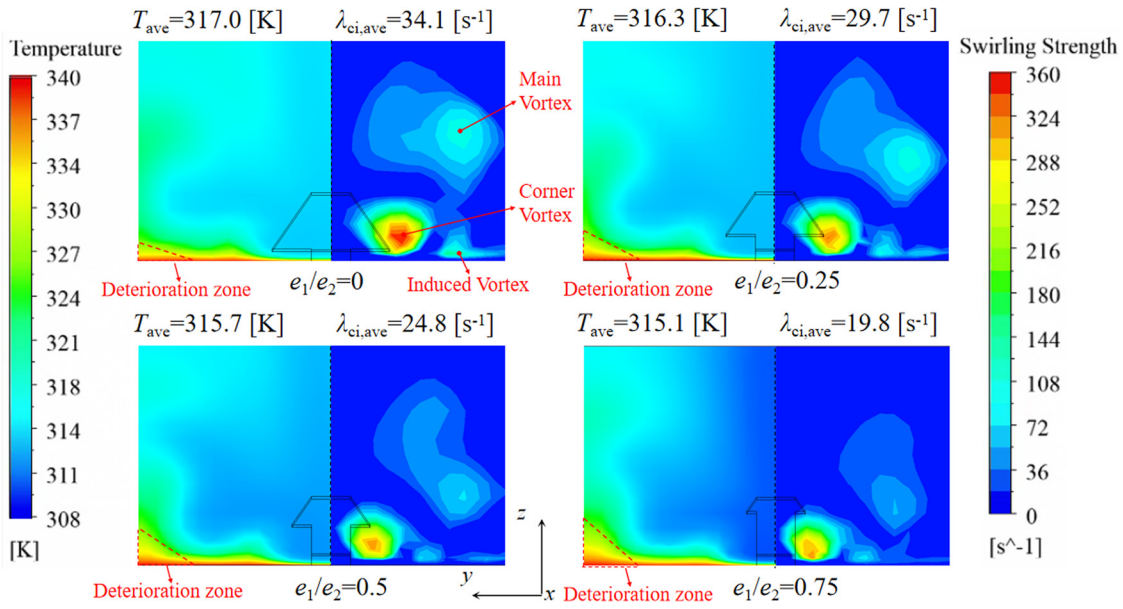

Figure 14: Temperature (left) and vortex intensity (right) distributions at *yz* plane (x = 772 mm) in the SDITW channel with different relative separation heights (e_1/e_2) (Re = 10,250, p_l = 70 mm, α = 30°, and $e/(0.5H)$ = 0.3).

decreases, the cross-sectional average air temperature increases and temperature uniformity improves. Furthermore, the triangular region in the left lower corner of Figure 14 indicates a high-temperature region, which is a flow deterioration region formed by the movement of the hot fluid from the wall to the core region. The collision of two adjacent transverse vortices near the wall causes flow deterioration, resulting in fluid momentum loss and heat transfer degradation. As the e_1/e_2 decreases, the induced vortex in the edge region is strengthened, which can reduce the fluid momentum loss and the heat transfer deterioration effect, and narrow the deterioration region.

Figure 15 shows the effects of relative separation height (e_1/e_2) and longitudinal pitch (p_l) of SDITW channel on the Nusselt number ratio (Nu/Nu_0), friction factor ratio (f/f_0), and PEC. As e_1/e_2 decreases, both the Nu/Nu_0 and f/f_0 increase, which means that the heat transfer enhancement is improved and the pressure loss is increased. A smaller e_1/e_2 represents a larger projected area and transverse span of the vortex generator, which can enhance the disturbance and vortex intensity in the fluid, thereby increasing the convective heat transfer and the pressure loss. Moreover, the Nu/Nu_0 and f/f_0 increase with the decrease in p_l. As p_l decreases, the fluid disturbance per unit length increases, and the longitudinal vortex in the SDITW channel is enhanced, which will enhance the heat transfer and increase pressure losses. It is observed that a decrease in p_l from 50 to 40 mm will lead to a small increase in the heat transfer enhancement of the SDITW channel, but a large increase in pressure loss. Therefore, p_l should not be too small. Furthermore, Figure 15(c) shows that the variation in PEC in SDITW channel is complex at different p_l and e_1/e_2. When p_l = 70 mm, the PEC variation with e_1/e_2 is insignificant, the PEC value is relatively high and its overall heat transfer performance is better.

4.2.2 Effect of blockage ratio and inclination angle

Figure 16 presents the temperature and vortex intensity distributions at *yz* plane (x = 772 mm) in the SDITW channel with various blockage ratios ($e/(0.5H)$) and inclination angles (α) at Re = 10,250, e_1/e_2 = 0, and p_l = 70 mm. As shown in Figure 16(a), when $e/(0.5H)$ = 0.3, both the maximum vortex intensity and the vortex influence range in the cross-section decrease as α increase, while the variation of average vortex intensity is small. When α increases, the position of the vortex changes, with the corner and induced vortex shifting towards the centerline, while the main vortex moving towards the lower right corner. When α reaches 60°, three vortices merge into a single large vortex. Furthermore, as α increases, the airflow temperature uniformity deteriorates and the average temperature decreases. The vortex locations can affect the airflow average temperature in the cross-section, even though the average vortex intensity is comparable for α = 20° and 60°. The convective heat transfer is improved due to the stronger vortex near the wall at α = 20°, while it is weakened by the weaker vortex near the wall at α = 60°. As shown in Figure 16(b), when $e/(0.5H)$ = 0.6, the cross-section averaged vortex intensity increases and the vortex

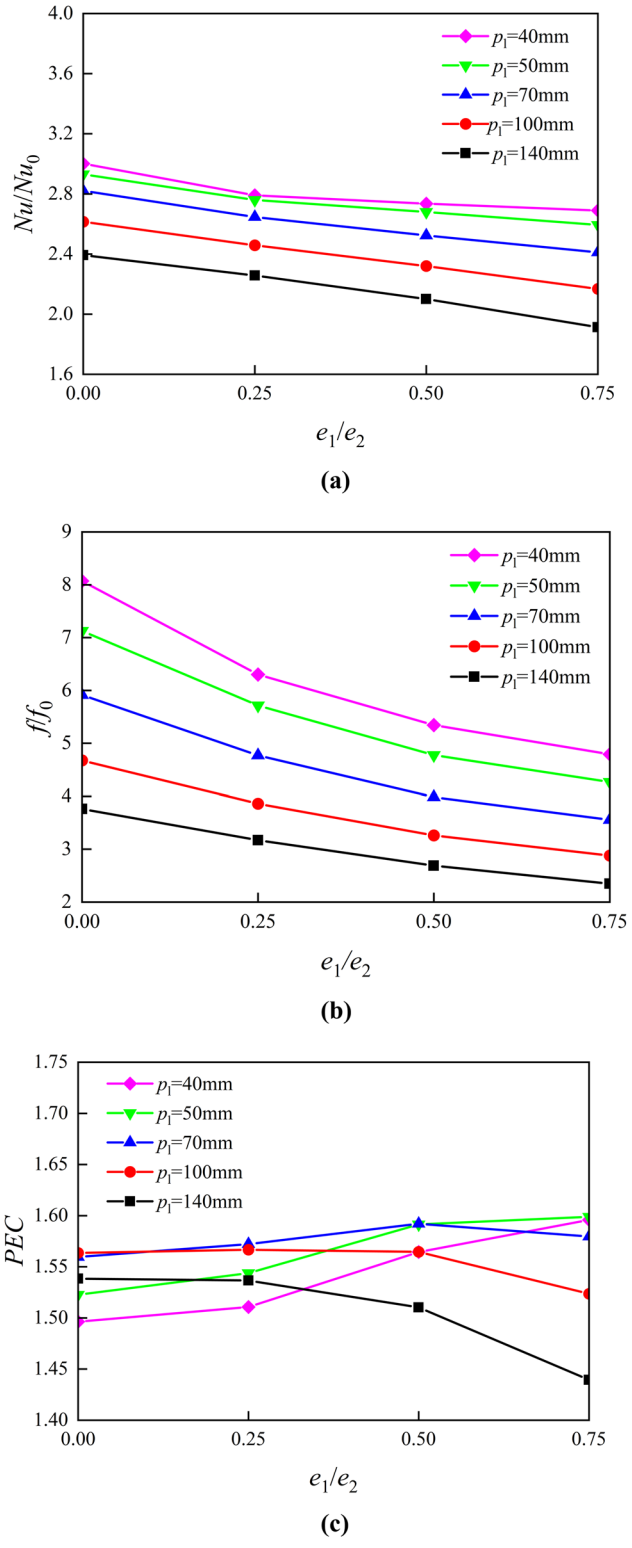

Figure 15: Variations in Nu/Nu_0, f/f_0, and PEC with relative separation height (e_1/e_2) and longitudinal pitch (p_l) in the SDITW channel (Re = 10,250, α = 30°, $e/0.5H$ = 0.3). (a) Nu/Nu_0. (b) f/f_0. (c) PEC.

influence range expands as α increases. There is a significant difference in the local vortex intensity in the near-wall region at different α. The local vortex intensity is maximum when α is 40° and minimum when α is 20°. Consequently, the convective heat transfer near the wall is the best when α is 40°, where airflow average temperature is the highest and the temperature distribution is most uniform in the cross-section. On the contrary, the heat transfer is the worst when α is 20°, where the airflow average temperature is the lowest and the temperature distribution is not uniform. Comparison of Figure 16(a) and (b) reveals that the effect of $e/(0.5H)$ on the vortex intensity and the temperature distribution in the SDITW channel varies with α. When α is relatively large, the effect of $e/(0.5H)$ is significant.

Figure 17 shows the effects of blockage ratios ($e/(0.5H)$) and inclination angles (α) in the SDITW channel on the Nusselt number ratio (Nu/Nu_0), friction factor ratio (f/f_0), and PEC. As shown in Figure 17(a), the variation trend of Nu/Nu_0 with $e/(0.5H)$ is different under different α. When α = 50° and 60°, Nu/Nu_0 increases with $e/(0.5H)$, indicating that a higher blockage ratio is beneficial for the heat transfer enhancement in the SDITW channel at large inclination angles. In contrast, when α = 20°–40°, Nu/Nu_0 first increases and then decreases with the increase in $e/(0.5H)$, suggesting that there exists an optimum $e/(0.5H)$ in this range of α, which will maximize the heat transfer enhancement in the SDITW channel. Furthermore, the sensitivity in SDITW channel caused by $e/(0.5H)$ will diminish as α decreases. When α = 20°, the variation in Nu/Nu_0 is minimum. As shown in Figure 17(b), f/f_0 increases with the increase in $e/(0.5H)$ at different α, which indicates that the flow resistance in SDITW channel increases. The increment of f/f_0 varies with α, and it is small when α is small. As shown in Figure 17(c), when α changes from 30° to 60°, the PEC of SDITW channel increases first and then decreases with the increase in $e/(0.5H)$, implying that there exists an optimum $e/(0.5H)$ value, which will lead to the highest PEC for this range of α. The PEC of SDITW channel is maximum at $e/(0.5H)$ = 0.3 at Re = 10,250 and α = 30°–60°, where the overall heat transfer performance of SDITW channel is the best.

5 Conclusion

In this study, the flow and heat transfer characteristics of SDITW vortex generator in a closed channel on the air-side

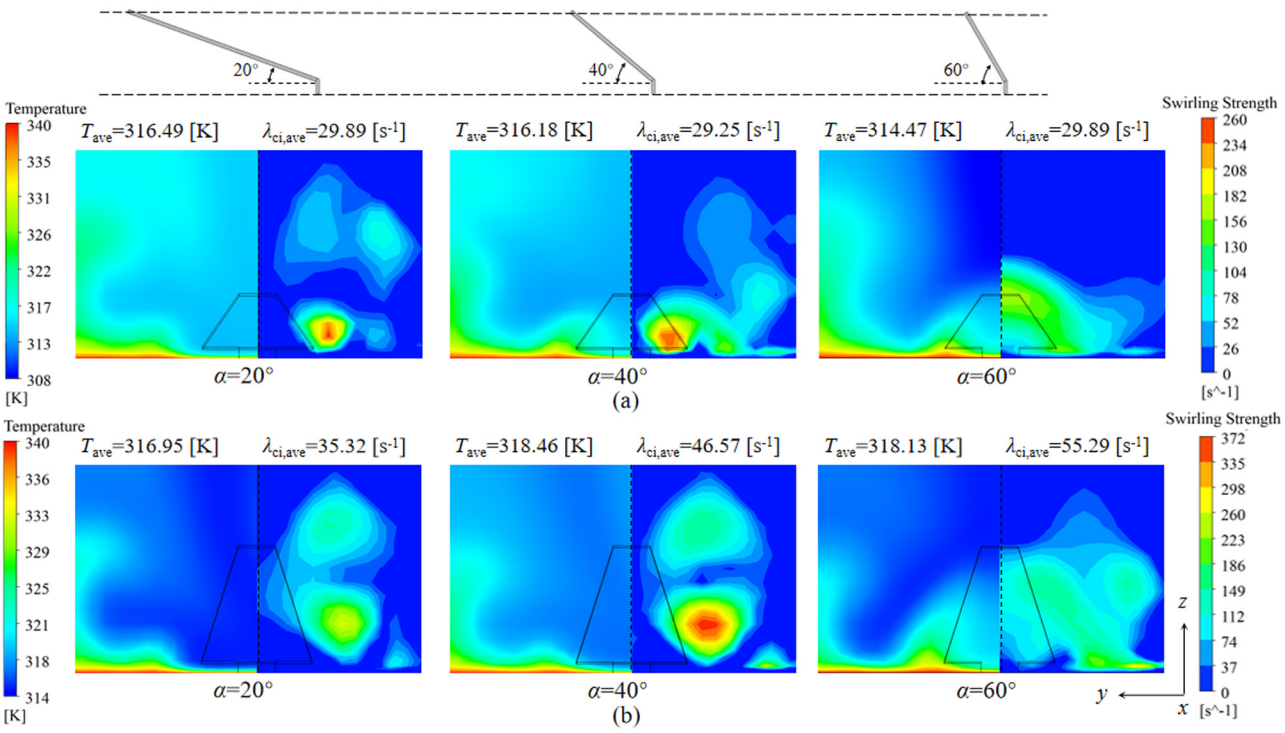

Figure 16: Temperature (left) and vortex intensity (right) distributions at *yz* plane (x = 772 mm) in the SDITW channel with different blockage ratios (e/(0.5H)) and inclination angles (α) (Re = 10,250, e_1/e_2 = 0, p_l = 70 mm). (a) e/(0.5H) = 0.3. (b) e/(0.5H) = 0.6.

of the panel-type radiator used for transformer were numerically investigated. The performance of SDITW was compared with that of IDW and ITW channels under the same geometric configuration. The effects of SDITW relative separation height (e_1/e_2), longitudinal pitch (p_l), blockage ratio (e/(0.5H)), and inclination angle (α) on the flow and heat transfer in the SDITW channel were analyzed in detail. The major findings are as follows:

1) Among the three vortex generators, SDITW has the highest local vortex intensity, followed by ITW and IDW. A stronger longitudinal vortex is formed in the SDITW channel as compared with IDW and ITW. On the other hand, more transverse vortices are created behind IDW and ITW. The semi-detached structure of SDITW can diminish the transverse vortices and flow resistance.
2) For Re = 5,125–15,375, the heat transfer enhancement (Nu/Nu_0) of ITW is 12.6–15.69% higher than that of IDW, while the pressure loss (f/f_0) is 39.1–48.3% higher. The heat transfer enhancement (Nu/Nu_0) of SDITW is 7.4–17.5% higher than that of IDW, while the pressure loss (f/f_0) is 21.9–25.7% higher. Therefore, the overall heat transfer performance (PEC) of SDITW is 0.5–8.9% higher than that of IDW and 1.7–4.9% higher than that of ITW.
3) For the same e/(0.5H) and α, the vortex intensity and influence range increase in the SDITW channel as e_1/e_2 decreases. As p_l decreases, the longitudinal vortex in the SDITW channel strengthens, the heat transfer performance improves, and the pressure loss increases. Both Nu/Nu_0 and f/f_0 of the SDITW channel increase as e_1/e_2 and p_l decrease. The PEC of SDITW channel is relatively high and its overall heat transfer performance is better when p_l = 70 mm.
4) For the same e_1/e_2 and p_l, the vortex intensity and influence range in the SDITW channel decrease as α increases when e/(0.5H) is 0.3, and its heat transfer performance deteriorates. When e/(0.5H) is 0.6, the vortex intensity and influence range in the SDITW channel increase as α increases, but its heat transfer is the best when α is 40° due to the difference in local vortex intensity near the wall region. For Re = 10,250 and α = 30°–60°, the PEC of the SDITW channel is maximum when e/(0.5H) = 0.3, and the overall heat transfer performance of the SDITW channel is the best.

The results obtained in the present study is meaningful in revealing the mechanism of flow resistance reduction and heat transfer enhancement for SDITW in a closed channel on the air side of a panel-type radiator used for

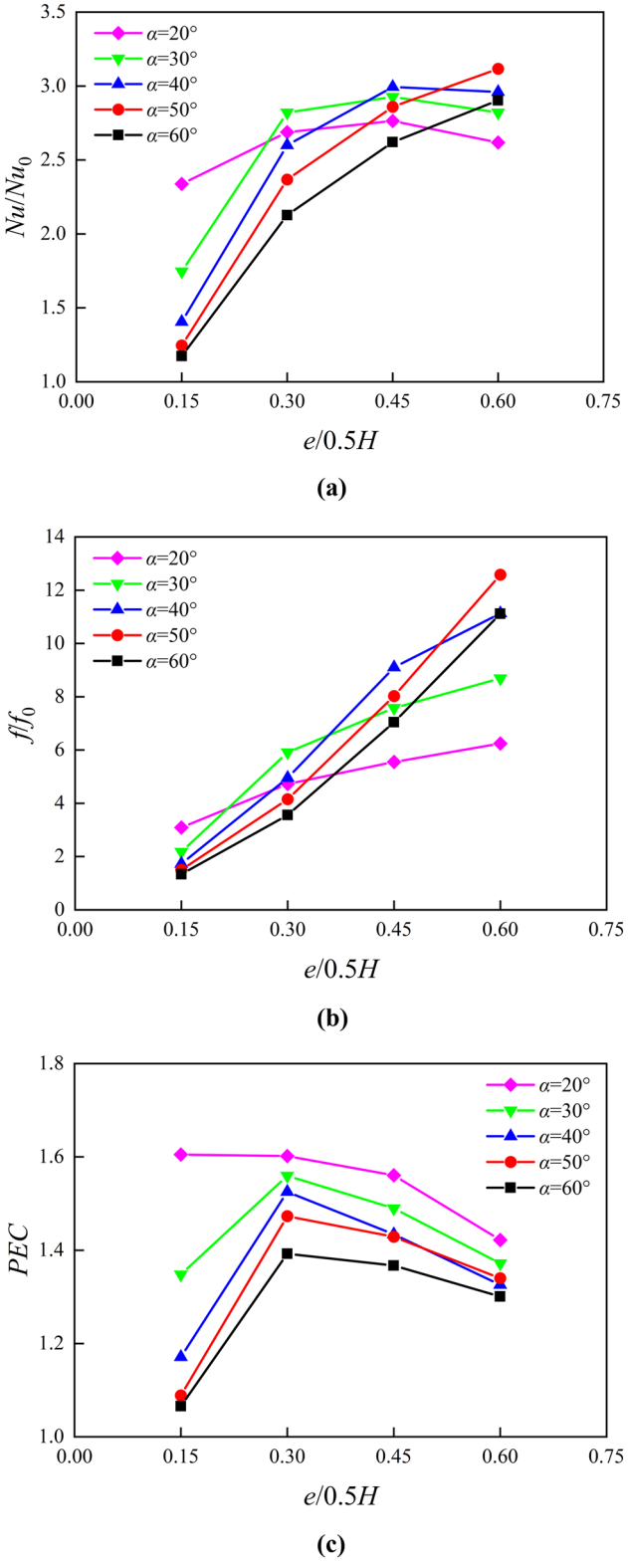

Figure 17: Variations in Nu/Nu_0, f/f_0, and PEC with blockage ratio ($e/(0.5H)$) and inclination angle (α) in the SDITW channel (Re = 10,250, e_1/e_2 = 0, and p_l = 70 mm). (a) Nu/Nu_0. (b) f/f_0. (c) PEC.

transformer. It can also provide a useful reference for the optimal design of vortex generator and corresponding heat dissipation channel for subsequent researchers.

Funding information: This work was supported by the S&T project of State Grid Shanghai Municipal Electrical Power Company under grant number 52094022000Y.

Author contributions: All authors have accepted responsibility for the entire content of this manuscript and approved its submission.

Conflict of interest: The authors state no conflict of interest.

Data availability statement: The data that support the findings of this study are available from the corresponding author upon reasonable request.

References

[1] Fiebig M. Embedded vortices in internal flow: heat transfer and pressure loss enhancement. Int J Heat Fluid Flow. 1995;16(5):376–88.
[2] Tiggelbeck S, Mitra NK, Fiebig M. Comparison of wing-type vortex generators for heat transfer enhancement in channel flows. J Heat Transf. 1994;116(4):880–5.
[3] Fiebig M, Kallweit P, Mitra N, Tiggelbeck S. Heat transfer enhancement and drag by longitudinal vortex generators in channel flow. Exp Therm Fluid Sci. 1991;4(1):103–14.
[4] Skullong S, Promthaisong P, Promvonge P, Thianpong C, Pimsarn M. Thermal performance in solar air heater with perforated-winglet-type vortex generator. Sol Energy. 2018;170:1101–17.
[5] Promvonge P, Skullong S. Enhanced heat transfer in rectangular duct with punched winglets. Chin J Chem Eng. 2020;28(3):660–71.
[6] Zhou G, Ye Q. Experimental investigations of thermal and flow characteristics of curved trapezoidal winglet type vortex generators. Appl Therm Eng. 2012;37:241–8.
[7] Lu G, Zhou G. Numerical simulation on performances of plane and curved winglet – Pair vortex generators in a rectangular channel and field synergy analysis. Int J Therm Sci. 2016;109:323–33.
[8] Min C, Qi C, Kong X, Dong J. Experimental study of rectangular channel with modified rectangular longitudinal vortex generators. Int J Heat Mass Transf. 2010;53(15):3023–9.
[9] Dogan M, Erzincan S. Experimental investigation of thermal performance of novel type vortex generator in rectangular channel. Int Commun Heat Mass Transf. 2023;144:106785.
[10] Demirağ HZ, Doğan M, İğci AA. The experimental and numerical investigation of novel type conic vortex generator on heat transfer enhancement. Int J Therm Sci. 2023;191:108383.
[11] Menni Y, Ameur H, Yao SW, Amine Amraoui M, Inc M, Lorenzini G, et al. Computational fluid dynamic simulations and heat transfer

characteristic comparisons of various arc-baffled channels. Open Phys. 2021;19(1):51–60.
[12] Promvonge P, Tongyote P, Skullong S. Thermal behaviors in heat exchanger channel with V-shaped ribs and grooves. Chem Eng Res Des. 2019;150:263–73.
[13] Skullong S, Promvonge P, Thianpong C, Pimsarn M. Thermal performance in solar air heater channel with combined wavy-groove and perforated-delta wing vortex generators. Appl Therm Eng. 2016;100:611–20.
[14] Promvonge P, Promthaisong P, Skullong S. Experimental and numerical thermal performance in solar receiver heat exchanger with trapezoidal louvered winglet and wavy groove. Sol Energy. 2022;236:153–74.
[15] Hu D, Zhang Q, Song K, Gao C, Zhang K, Su M, et al. Performance optimization of a wavy finned-tube heat exchanger with staggered curved vortex generators. Int J Therm Sci. 2023;183:107830.
[16] Min C, Jin J, Wang X, Qi C. Numerical investigation of natural convection heat transfer for panel type radiator mounted with longitudinal vortex generators. ICMREE 2011: Proceedings of the 2011 International Conference on Materials for Renewable Energy and Environment; 2011 May 20–22. Shanghai, China, New York: IEEE; 2011. p. 1267–70.
[17] Garelli L, Ríos Rodriguez G, Dorella JJ, Storti MA. Heat transfer enhancement in panel type radiators using delta-wing vortex generators. Int J Therm Sci. 2019;137:64–74.
[18] Rodriguez GR, Garelli L, Storti M, Granata D, Amadei M, Rossetti M. Numerical and experimental thermo-fluid dynamic analysis of a power transformer working in ONAN mode. Appl Therm Eng. 2017;112:1271–80.
[19] Nabati H, Mahmoudi J, Ehteram A. Heat transfer and fluid flow analysis of power transformer's cooling system using CFD approach. Chem Prod Process Model. 2009;4(43):1–16.
[20] Xiao H, Dong Z, Liu Z, Liu W. Heat transfer performance and flow characteristics of solar air heaters with inclined trapezoidal vortex generators. Appl Therm Eng. 2020;179:115484.
[21] Bekele A, Mishra M, Dutta S. Performance characteristics of solar air heater with surface mounted obstacles. Energy Convers Manag. 2014;85:603–11.
[22] Yu C, Zhang H, Wang Y, Wang J, Gao B, Fang Z. Comparative study of the thermal performance of four different parallel flow shell and tube heat exchangers with different performance indicators. Open Phys. 2020;18(1):1121–35.
[23] Oneissi M, Habchi C, Russeil S, Bougeard D, Lemenand T. Novel design of delta winglet pair vortex generator for heat transfer enhancement. Int J Therm Sci. 2016;109:1–9.
[24] Habchi C, Oneissi M, Russeil S, Bougeard D, Lemenand T. Comparison of eddy viscosity turbulence models and stereoscopic PIV measurements for a flow past rectangular-winglet pair vortex generator. Chem Eng Process. 2021;169:108637.
[25] Lotfi B, Sundén B, Wang Q. An investigation of the thermo-hydraulic performance of the smooth wavy fin-and-elliptical tube heat exchangers utilizing new type vortex generators. Appl Energy. 2016;162:1282–302.
[26] Menter F. Review of the shear-stress transport turbulence model experience from an industrial perspective. Int J Comut Fluid Dyn. 2009;23:305–16.
[27] Dogan M, Abir İgci A. An experimental comparison of delta winglet and novel type vortex generators for heat transfer enhancement in a rectangular channel and flow visualization with stereoscopic PIV. Int J Heat Mass Transf. 2021;164:120592.
[28] Incropera FP, Dewitt DP, Bergman TL, Lavine AS. Fundamentals of heat mass transfer. John-Wiley Sons; 2006.
[29] Zhou J, Adrian R, Balachandar S, Kendall TM. Mechanisms for generating coherent packets of hairpin vortices in channel flow. J Fluid Mech. 1999;387:353–96.
[30] Lee SJ, Lee S, Hassan YA. Numerical investigation of turbulent flow in an annular sector channel with staggered semi-circular ribs using large eddy simulation. Int J Heat Mass Transf. 2018;123:705–17.